RSC Advances

PAPER

View Article Online
View Journal | View Issue

Cite this: *RSC Adv.*, 2017, **7**, 32146

Mn/SAPO-34 as an efficient catalyst for the low-temperature selective catalytic reduction of NO_x with NH_3

Chengkai Pang, Yuqun Zhuo* and Qiyu Weng

A series of Mn-exchanged SAPO-34 catalysts were synthesized and developed as catalysts for the low temperature selective catalytic reduction (SCR) of NO with ammonia in the presence of excess oxygen. 4Mn/SAPO-34 showed the highest SCR activity in the temperature range of 120–210 °C. The microstructure of zeolite supports, acidity, manganese species and reaction mechanism were investigated in detail by BET, NH_3-TPD, UV-Vis, H_2-TPR, XPS and *in situ* DRIFTS. Mn^{3+} and Mn^{4+} related species were proved to be the active sites for the SCR reaction. The Eley–Rideal mechanism was proved to be effective on 4Mn/SAPO-34 for the low temperature SCR reaction in which coordinated NH_4^+ species react with gas-phase NO to form an activated transition state and subsequently decomposed to N_2 and H_2O.

Received 8th May 2017
Accepted 16th June 2017

DOI: 10.1039/c7ra05165d

rsc.li/rsc-advances

1. Introduction

Nitrogen oxides, including NO, NO_2 and N_2O have long been considered as the major source of air pollution causing photochemical smog, acid rain, ozone depletion and the greenhouse effect. One of the most effective techniques to eliminate NO_x pollution is SCR technology with ammonia as the reductant ($4NO + 4NH_3 + O_2 \rightarrow 4N_2 + 6H_2O$). The commercial SCR catalyst V_2O_5–$MoO_3(WO_3)/TiO_2$ only works efficiently under 300–400 °C. However, for many industrial applications, such as cement plants, iron and steel plants, especially gas-fired boilers, the suitable process temperature to arrange NO_x removal is usually below 200 °C, thus making it necessary to develop low temperature SCR catalysts to avoid reheating of the flue gas and reduce cost.

Many metal oxide catalysts have long been investigated for the low-temperature SCR reaction, such as MnO_x–CeO_x,[1,2] Mn–Ce–Ti mixed-oxide,[3] W–Mn–Zr mixed-oxide,[4] Ni–Mn/TiO_2.[5] These researchers had attributed the excellent SCR activity to Mn^{3+} and Mn^{4+} species. The most recent SCR catalyst formulations contain copper exchanged into the chabazite (CHA) family of zeolites. Cu-SSZ-13 (ref. 6) and Cu-SAPO-34 (ref. 7 and 8) catalysts attracted much attention for their utility in NH_3–SCR reactions and had demonstrated good low-temperature SCR activity and hydrothermal stability.

Besides high surface area and good hydrothermal stability, SAPO-34 can offer many acid sites of different strength which are important to SCR activity, but Mn–M/TiO_x (M = Ce, Fe, *etc.*) catalysts usually lack of, therefore manganese oxides catalyst with SAPO-34 as the carrier might show good low temperature SCR activity.

In terms of the reaction mechanism, two still-under-debate mechanism have been proposed for the low-temperature SCR, some agree that the Eley–Rideal mechanism occurs, *i.e.* the gaseous NO react with activated NH_3 species to an activated transition state and subsequently decomposed to N_2 and H_2O;[8,9] and some claim the Langmuir–Hinshelwood mechanism occurs, *i.e.* adsorbed NO or NO_2 species react with adsorbed NH_3 species on the adjacent sites, followed by reaction to an activated transition state and decomposition to the reaction products.[10,11]

In the present work, the treatment of exhaust from gas-fired boiler which contains high concentration of H_2O and very low concentration of SO_2 is focused. So *x*Mn/SAPO-34 ($x = 1, 2, 4, 8$) was developed as a new catalyst for low temperature SCR with NH_3. With the characterization of H_2-TPR, XPS and UV-Vis, the active site could be determined. Furthermore, the SCR mechanism on Mn/SAPO-34 was investigated by *in situ* DRIFTS study.

2. Experimental

2.1 Catalyst preparation

The ion-exchanged *x*Mn/SAPO-34 ($x = 1, 2, 4, 8$) catalyst was prepared by liquid ion-exchange method. First in order to avoid poison of catalysts from alkali metal which decrease catalytic activity for low temperature SCR reaction, commercial Na-SAPO-34 powder (Jiangsu XFNANO) was converted to NH_4/SAPO-34 by ion exchange with NH_4Cl (Aladdin, purity > 98.5%) solution. Then Mn ion-exchange was performed by mixing NH_4/SAPO-34 with different concentration of $Mn(NO)_2$ (Across, purity > 95%)

Key Laboratory for Thermal Science and Power Engineering of Ministry of Education, Beijing Engineering Research Center for Ecological Restoration and Carbon Fixation of Saline-alkaline and Desert Land, Department of Thermal Engineering, Tsinghua University, Beijing 100084, China. E-mail: zhuoyq@tsinghua.edu.cn

solution at 80 °C for 6 h under vigorously stirring. Then it was dried in rotary evaporator and in an oven at 110 °C for 16 h and finally *x*Mn/SAPO-34 ($x = 1, 2, 4, 8$) was obtained by calcination in the gas of 21% O_2/N_2 at 550 °C for 3 h.

2.2 NH_3 SCR activity measurements

The catalytic activity evaluation was carried out using a flow-through powder reactor system equipped with a Fourier Transform Infrared (FT-IR) spectrometer (THERMO SCIENTIFIC IGS) with a gas-sampling cell. Fig. 1 shows the schematic diagram of experimental apparatus.

In order to prevent condensation along upstream tubing, all the gas lines were heated and maintained at 120 °C. The gas mixture for the NH_3-SCR reaction consisted of 500 ppm NO, 500 ppm NH_3, 16.3% vol. H_2O (if in the water resistance test) and 3% vol. O_2 balanced with N_2. The gas hourly space velocity (GHSV) was 65 000 h^{-1} for the standard SCR. Prior to the activity measurements, the catalysts were pretreated at 500 °C and held for 30 min in 21% vol. O_2/N_2 flow. The catalytic activities were measured at the temperature range of 120–210 °C. The typical time to achieve steady state at each temperature was about 2.5 h. The NO conversions were calculated based on the inlet and outlet gas concentrations at steady state by the following equation:

$$\text{NO conversion} = \frac{C_{\text{NO}_{x\text{in}}} - C_{\text{NO}_{x\text{out}}}}{C_{\text{NO}_{\text{in}}}} \times 100\% \quad (1)$$

$$\text{N}_2 \text{ selectivity} = \left(1 - \frac{2[\text{N}_2\text{O}]_{\text{outlet}}}{[\text{NO}_x]_{\text{inlet}} - [\text{NO}_x]_{\text{outlet}}}\right) \times 100\% \quad (2)$$

2.3 Characterization

X-ray diffraction patterns were collected on a bruker D8 Advance X-ray diffractometer with a Ni-Filtered Cu Kα with a step size of 0.02 in the 2θ range from 5° to 40°.

The ammonia temperature programmed desorption (NH_3-TPD) experiment was carried out in quartz tube reactor equipped with a Fourier Transform Infrared (FT-IR) spectrometer (THERMO SCIENTIFIC IGS) with a gas-sampling cell. 150 mg of prepared samples were firstly pretreated in 21% vol. O_2/N_2 at 500 °C for 30 min. Then a total flow of 100 ml min^{-1} containing 2500 ppm NH_3 in N_2 was injected into the reactor for 2 hours to achieve steady state. Once the catalyst was saturated, NH_3 was switched off and the catalyst was swept by N_2 overnight to remove any gas phase NH_3. Finally the catalyst was heated in N_2 at a temperature ramp to 700 °C with a heating rate of 10 °C min^{-1}.

The manganese contents were determined by coupled plasma (ICP) optical emission spectroscopy (Thermo IRIS Intrepid II) of dissolutions of the ground catalysts in acid solutions.

The BET surface area, pore volume and pore size of samples were measured by N_2 adsorption using a MICROMERITICS ASAP 2020 surface area and porosity analyzer.

Diffuse reflectance UV-Vis spectra were recorded in the range of 200–800 nm against a $BaSO_4$ reference standard on a HitachiU-300 UV-Vis-NIR spectrophotometer equipped with an integration sphere.

The H_2-TPR experiments were performed on a custom made setup using 20 mg of calcined catalyst. The catalysts were pretreated at 500 °C for 30 min in a highly pure O_2 (40 ml min^{-1}) stream to renew the samples and make sure the surface was clean. The furnace temperature was lowered to room temperature in N_2, and then the feed containing 5% vol. H_2 in N_2 was fed at a flow rate of 40 ml min^{-1}. H_2-TPR runs were performed by heating the samples from room temperature to 800 °C at a linear heating rate of 10 °C min^{-1} and finally keeping the temperature constant for 30 min at 800 °C to ensure complete metal oxide reduction. The hydrogen consumed in the TPR was measured by a TCD.

X-ray photoelectron spectroscopy (XPS) analyses were performed on a PHI quantera SXM Scanning ESCA Microprobe (Physical Electronics) with a hemispherical detector operating at constant pass energy (PE = 55 eV) using Al Kα radiation (1486.6 eV). All binding energies were referenced to the C 1s line at 284.8 eV.

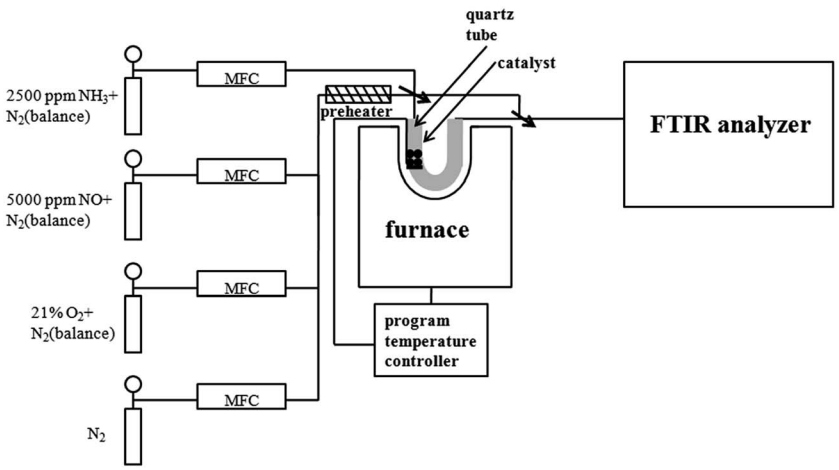

Fig. 1 Schematic diagram of experimental apparatus for activity test.

Diffuse reflectance infrared Fourier transform spectra (DRIFTS) were measured on a FT-IR spectrometer (Thermo Nicolet NEXUS870) with a MCT detector and a high temperature reaction chamber (Harrick Scientific Praying Mantis) with ZnSe windows, which was connected to a gas-dosing system. The oxidation pretreatments at 500 °C for 1 h were executed to remove the adsorbed water and clean the surface before each measurement. The DRIFTS spectra were recorded in the range of 4000–650 cm^{-1} for 32 scans with a resolution of 4 cm^{-1}. The background spectra were collected for 32 scans with a resolution of 4 cm^{-1} before exposed to the absorbates.

3. Results and discussion

3.1 Effect of Mn loading on NH_3 SCR activity

In low temperature SCR experiments, the NO_x and NH_3 conversions were tested as a function of steady temperature (ranging from 120 to 210 °C) over *x*Mn/SAPO-34 catalysts. Fig. 2a shows the NO conversion profile of *x*Mn/SAPO-34 ($x = 1, 2, 4, 8$) catalysts. The maximum NO conversion of NH_4/SAPO-34 is about 20%, which is consistent with the previous results on H-ZSM-5, H-BETA and H-SSZ-13, where the proton form zeolite was not very active for standard SCR reaction.[12,13] Compared with Mn/SAPO-34 catalysts, NH_4/SAPO-34 does not have much catalytic activity in the whole temperature range (120–210 °C), indicating that the Mn species could be of the great importance to the SCR activities.

When Mn loading increased from 1% to 4%, the catalytic activity increased significantly from 26% to 82% at 180 °C. When Mn loading increased to 8%, catalytic activity drops to 58% at 180 °C, this might be caused by the blockage of micro pores and the decrease of exposed manganese due to the aggregation of manganese oxides.

Compared with other researches, Lei Ma[14] reported that for H_2O resistance test, the SCR activity of Cu-SAPO-34 catalyst at 150 °C was about 30% when GHSV = 30 000 h^{-1} and the concentration of NO and NH_3 was 350 ppm. So comparing with Cu-SAPO-34 Lei Ma had made, the Mn/SAPO catalyst showed much better SCR activity and H_2O tolerance. Boxiong Shen[15] reported that when GHSV = 5000 h^{-1} and the concentration of NO and NH_3 was 600 ppm, the SCR activity of Mn–Ce/Ti–PILCs prepared at 120 °C was 50%. Comparing with Mn–Ce/Ti–PILCs, the Mn/SAPO catalyst showed similar SCR activity while Ce was not added to increase SCR activity of Mn/SAPO yet.

Fig. 2b shows the NO conversion profile of the *x*Mn/SAPO-34 ($x = 1, 2, 4, 8$) catalysts of water resistance test. For 4Mn/SAPO-34 and 8Mn/SAPO-34 catalysts, the introduction of H_2O retard low temperature SCR reaction, while for 1Mn/SAPO and 2Mn/SAPO catalysts, the existence of H_2O in the gas phase improve the catalytic activity except for 120 °C. It might be explained that the introduction of H_2O might change the environment of Mn ions or generate acid sites that help increase SCR activity besides covering active sites as A. Lorena Picone *etc.*[16] found the introduction of H_2O increased the SCR activity of Cu-SAPO STA-7(IE) and Raquel Martínez-Franco[17] found the hydrothermal treatment could increase the SCR activity of Cu-SAPO-34.

The concentration of generated NO_2 was below 30 ppm and there was almost no N_2O generated, according to eqn (2), the selectivity was almost 100% in the temperature range of 120–210 °C, so it is beyond discussion.

3.2 XRD

Fig. 3 shows the XRD patterns of *x*Mn/SAPO-34 with different Mn loadings. XRD is commonly used for detection of metal or metal oxides phase. As shown in Fig. 3, the diffraction peaks of *x*Mn/SAPO-34 exhibit chabazite phase with space group of $R\bar{3}m$. This observation agrees well with those of SAPO-34,[6,7] indicating the crystalline structure of SAPO-34 unchanged after catalyst preparation. As Mn loading of *x*Mn/SAPO-34 increased, no manganese oxide phase had been detected except for 8Mn/SAPO-34 in which two peaks belonging to MnO_2 appears, indicating the aggregation of manganese oxide on 8Mn/SAPO-34. This is also supported by BET surface area results. For other samples, the manganese oxide might be amorphous or too small to be detected.

3.3 Effect of Mn loading on surface area and pore characterization

As shown in Table 1, when Mn loading increased from 1 to 8%, BET surface area and micro pore volume decreased gradually,

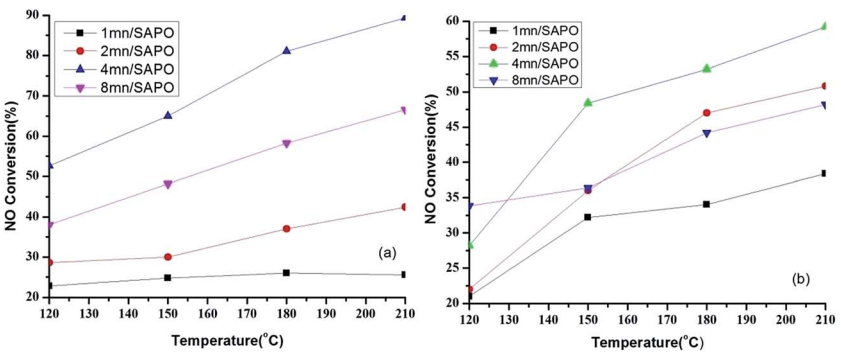

Fig. 2 Catalytic activity of *x*Mn/SAPO-34 ($x = 1, 2, 4, 8$) for low-temperature SCR of NO with NH_3. Conditions: (a) 500 ppm NO + 500 ppm NH_3 + 3% vol. O_2 + N_2 balanced, GHSV = 65 000 h^{-1}; (b) 500 ppm NO + 500 ppm NH_3 + 16.3% vol. H_2O + 3% vol. O_2 + N_2 balanced, GHSV = 65 000 h^{-1}.

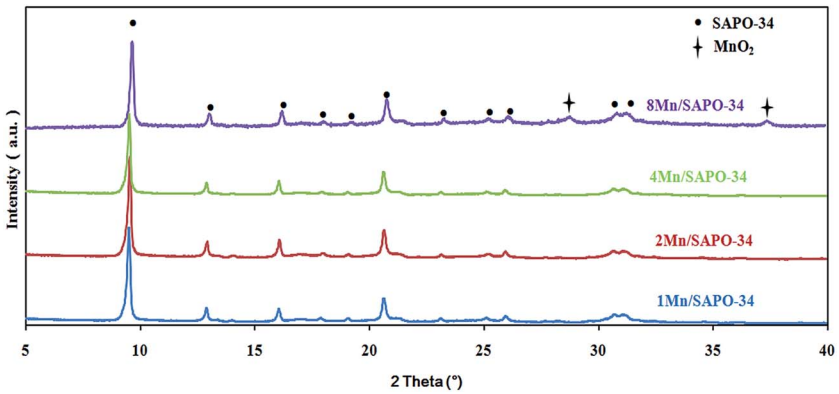

Fig. 3 XRD patterns of *x*Mn/SAPO-34 ($x = 1, 2, 4, 8$).

Table 1 Physico-chemical properties of *x*Mn/SAPO-34 ($x = 1, 2, 4, 8$)

Sample	BET surface area ($m^2\ g^{-1}$)	Micro pore volume ($cm^3\ g^{-1}$)	Micro pore diameter (nm)	Mn loading from ICP (%wt)
1Mn/SAPO-34	426	0.227	2.05	0.996
2Mn/SAPO-34	402	0.218	2.04	1.947
4Mn/SAPO-34	393	0.205	2.04	4.117
8Mn/SAPO-34	375	0.205	2.42	7.484

while micro pore diameter was almost the same except for 8Mn/SAPO-34 that it increased. According to XRD results, this might be caused by the blockage of micro pores due to the aggregation of manganese oxides.

The Mn loading was almost the same as the set values for each catalyst indicating the catalyst preparing process was acceptable.

3.4 NH_3-TPD

The NH_3-TPD can be used to study the acidity property of each sample in different temperature. Fig. 4 shows the effluent NH_3 profiles during NH_3-TPD process on each sample. As Mn loading increased, the desorption amount of NH_3 decreased, this could be explained by Mn ion exchange process in which Mn ions might replace H^+, leading to the decreasing of acid sites on catalysts. In Fig. 4, there were four NH_3 desorption peaks: a low temperature peak at 220 °C, two middle temperature peaks at 320 and 400 °C, and a high temperature peak at 500 °C. Different desorption peaks represent different NH_3 adsorption strength. Before 220 °C, the shapes of all the profiles were almost the same, while according to Fig. 2 the activities of these catalysts differ a lot, suggesting that these related NH_3 adsorption sites may not be involved in catalytic cycle or in another word, these adsorbed NH_3 were not well activated. This was supported by D. Wang *et al.*[18] that the appearance of the low temperature peak at about 200 °C was attributed to weakly adsorbed NH_3.

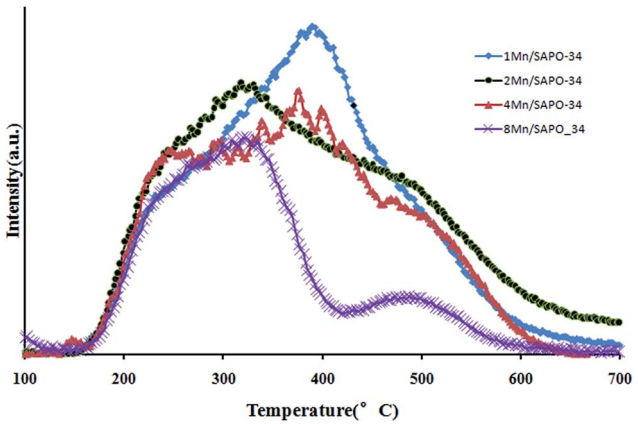

Fig. 4 NH_3-TPD of *x*Mn/SAPO-34 ($x = 1, 2, 4, 8$).

Whichever mechanism might dominate, NH_3 needs to be adsorbed and well activated, therefore, the interactions between NH_3 and catalyst surface cannot be too weak like those desorbed at 200 °C or too strong. According to Fig. 1, the catalysis activity increased as Mn loading increased from 1% to 4%, while it dropped when Mn loading further increased to 8%. Since all the NH_3-TPD profiles were similar except that of 8Mn/SAPO-34, the different activity between 1Mn/SAPO-34, 2Mn/SAPO-34 and 4Mn/SAPO-34 could be ascribed to different Mn loading, while the decreased activity of 8Mn/SAPO might be ascribed to the decreased acid sites from which NH_3 desorbed at 400 and/or 500 °C. This indicated that the acid sites responsible for the NH_3 desorption at 400 °C or/and 500 °C were important to low temperature SCR reaction.

3.5 DR UV-Vis

Diffuse reflectance UV-Vis spectroscopy is the common characterization method for the determination of oxidation and coordination state of metal complexes on the out surface and in

the zeolite channels. Fig. 5 shows the UV-Vis spectra of all catalysts. The absorption bands of all samples at 240 nm were related to the charge transfer processes between framework aluminum and oxygen atoms of aluminophosphate and water molecules.[19] The broad band in the range 320–380 nm was attributed to $Mn^{3+} \leftarrow O^{2-}$ charge transfer transition superimposed on $^5B_{1g} \rightarrow {}^5B_{2g}$ crystal field d–d transition.[20] The band at 332 nm was tentatively assigned to $Mn^{3+} \leftarrow O^{2-}$ charge transfer in Mn_3O_4 in which manganese was octahedrally coordinated with oxygen.[21–23] The band at 255–276 nm could be assigned to the $Mn^{2+} \leftarrow O^{2-}$ charge transfer transition in tetrahedral oxygen coordination.[21,22] In the α-Mn_2O_3 structure, Mn^{3+} ions occupy octahedral sites, if highly symmetric, a single spin-allowed absorption band in the d–d transition region was expected similarly to $[Mn(H_2O)_6]^{3+}$ at 500 nm.

In Fig. 5 it showed there was a distinct difference between the spectra of 2Mn/SAPO-34 and 4Mn/SAPO-34, while the spectra of 1Mn/SAPO-34 and 2Mn/SAPO-34 were similar as well as that of 4Mn/SAPO-34 and 8Mn/SAPO-34. Specifically, when Mn loading increased from 2% to 4%, the band at 320–380 nm increased greatly, indicating the percentage of Mn^{3+} increased. Meanwhile the negative band at 255–276 nm emerged, indicating the percentage of Mn^{2+} decreased, which might be caused by partial oxidation of Mn^{2+} to Mn^{3+} or Mn^{4+} when Mn loading increased.

3.6 H_2-TPR

Fig. 6 presented the H_2-TPR profiles of four catalysts. H_2-TPR is commonly used for information on the oxidation state of metal oxides. For 4Mn/SAPO-34 and 8Mn/SAPO-34 catalysts, there were two sharp peaks respectively at about 350 °C and 440 °C, the former one indicated the reduction of Mn^{4+} to Mn^{2+}, and the latter one indicated the reduction of Mn^{3+} to Mn^{2+}.[23,24] For 1Mn/SAPO-34 and 2Mn/SAPO-34 catalysts, there was only a broad peak between 300–500 °C, indicating that most of the Mn species on these two catalysts were Mn^{2+} which could not be reduced below 700 °C. As indicated, there was a significant change when Mn loading increased from 2% to 4% that the Mn^{2+} species changed to Mn^{3+} and/or Mn^{4+} species. This result was consistent with UV-Vis results.

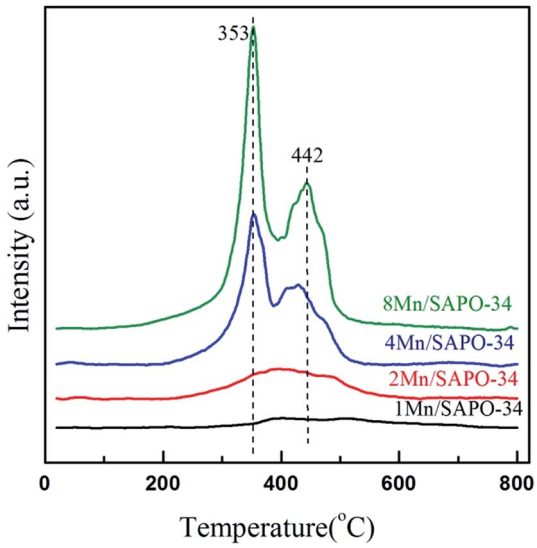

Fig. 6 H_2-TPR of xMn/SAPO-34 (x = 1, 2, 4, 8).

3.7 XPS

To investigate the surface chemical states of these catalysts, the XPS spectra of the Mn $2P_{3/2}$ were obtained, as shown in Fig. 7. Two main peaks respectively assigned to Mn $2P_{3/2}$ at 642.5 ev and Mn $2P_{1/2}$ at 654 ev were observed. Comparing with those reported for MnO, Mn_2O_3 and MnO_2,[25] the measured binding energy of Mn $2P_{3/2}$ in xMn/SAPO-34 (x = 1, 2, 4, 8) catalysts was slightly higher, it could be strong evidence that strong interactions existed between Mn species and SAPO-34 carrier.

By performing a peak-fitting deconvolution, Mn species could be separated into three peaks: 640.8–640.9 ev, 642.1–642.3 ev and 643.8–644.1 ev, which correspond to Mn^{2+}, Mn^{3+} and

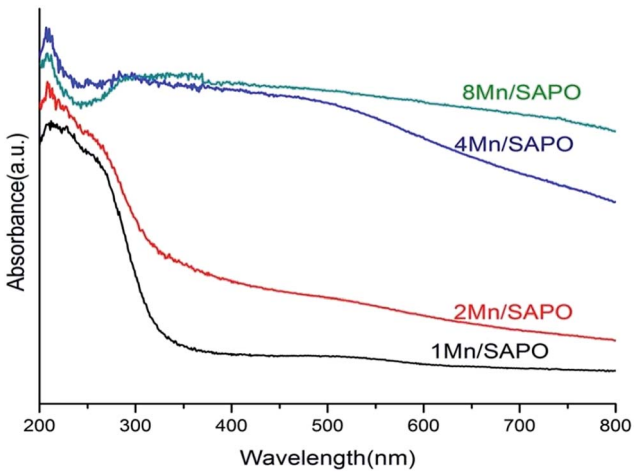

Fig. 5 DR UV-Vis spectra recorded under ambient atmosphere of xMn/SAPO-34 (x = 1, 2, 4, 8).

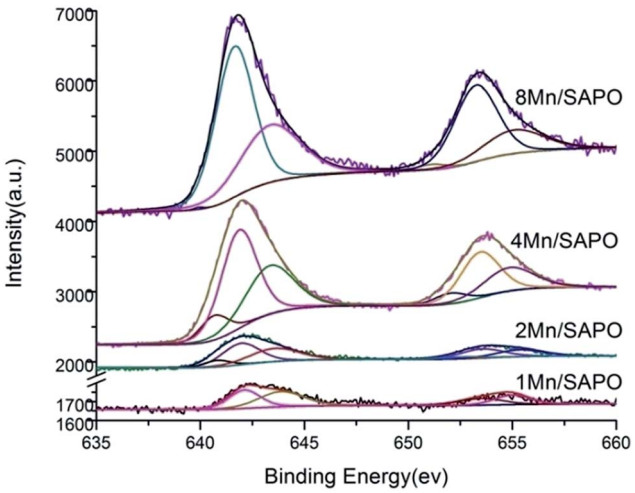

Fig. 7 XPS spectra for Mn 2P of the xMn/SAPO-34 (x = 1, 2, 4, 8) catalysts.

Table 2 Binding energies (ev) of core electrons of the *x*Mn/SAPO-34 (x = 1, 2, 4, 8) catalysts and the percentage of different valence state

	Mn^{2+}		Mn^{3+}		Mn^{4+}	
Compound	Peak (ev)	%	Peak (ev)	%	Peak (ev)	%
1Mn/SAPO-34	641.0	0.9	642.12	46.6	643.88	52.5
2Mn/SAPO-34	640.68	9.5	641.82	46.1	643.34	44.4
4Mn/SAPO-34	640.58	11.0	641.77	54.2	643.11	34.8
8Mn/SAPO-34	639.92	0.8	641.57	62.6	643.19	36.6

Mn^{4+} respectively. Table 2 had listed the atom percentage of Mn species in different valence state determined by XPS. As Mn loading increased, the percentage of Mn^{3+} increased while the percentage of Mn^{4+} decreased. This observation is quite different from that obtained from UV-Vis and H_2-TPR spectra. The could be explained that the information acquired from XPS spectra is about the element on the outer surface of the samples, since for XPS spectra, only the information of the element about 3λ depth below the surface (λ is the depth of several atoms) can be obtained, while H_2-TPR spectra reflect the characteristics of bulk phase and UV-Vis spectra reflect the

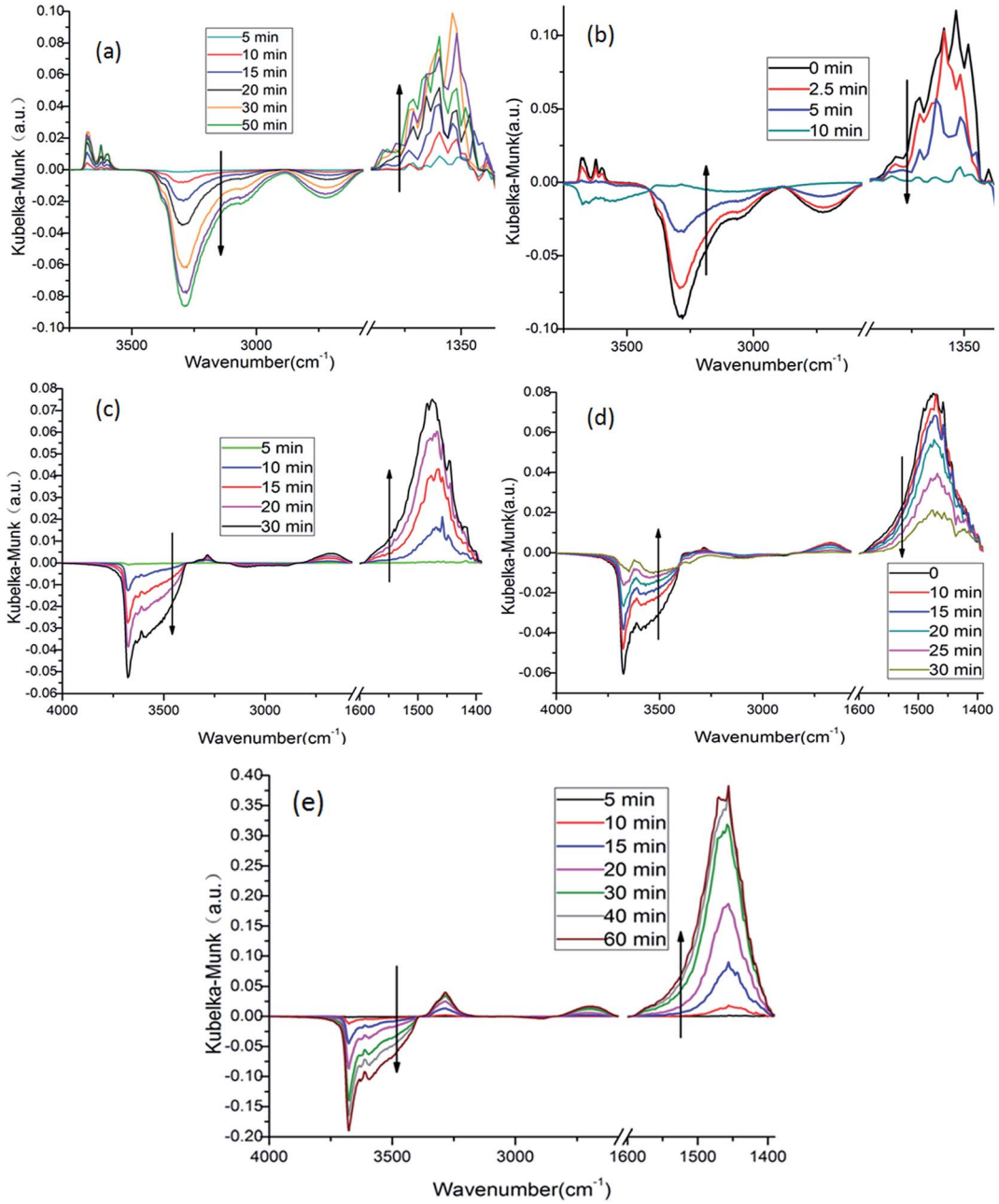

Fig. 8 DRIFTS spectra of 4Mn/SAPO-34 at 150 °C exposed to (a) 500 ppm NO + 3% vol. O_2 + N_2 (balance) (b) 500 ppm NH_3 + 3% vol. O_2 + N_2 (balance) after saturated with NO (c) 500 ppm NH_3 + 3% vol. O_2 + N_2 (balance) (d) 500 ppm NO + 3% vol. O_2 + N_2 (balance) after saturated with NH_3 (e) 500 ppm NO + 500 ppm NH_3 + 3% vol. O_2 + N_2 (balance).

characteristics of metal oxides species on the outer and inner surface especially in zeolite channels of catalyst.[26,27]

According to UV-Vis and H_2-TPR results, most of the Mn species on the surface of 1Mn/SAPO-34 and 2Mn/SAPO-34 were Mn^{2+}, while that of 4Mn/SAPO-34 and 8Mn/SAPO-34 were Mn^{3+}. The XPS spectra showed that, on outer surface of the samples, most of the Mn species were Mn^{3+} and Mn^{4+}. These results indicated that for 1Mn/SAPO-34 and 2Mn/SAPO-34, most of the Mn species are Mn^{2+}, the Mn species in the zeolite channels were Mn^{2+}, while that on the outer surface were Mn^{3+} and Mn^{4+}; for 4Mn/SAPO-34 and 8Mn/SAPO-34, most of the Mn species were Mn^{3+} and Mn^{4+}.

3.8 DRIFTS

3.8.1 NO adsorption and subsequent reaction with NH_3. In order to identify the adsorbed NO species, *in situ* DRIFTS was performed on catalysts exposed to 500 ppm NO with 3% vol. O_2 balanced by N_2 (100 ml min^{-1}). In Fig. 8a, there was only one positive band at about 1360 cm^{-1}, which belonged to nitrite groups.[28,29] There was no other detectable positive bands between 1200–1600 cm^{-1}, suggesting that the nitrite groups might be the only NO species. The negative bands at 3300 cm^{-1} and 2700 cm^{-1} might originate from the depletion of Brønsted base sites, *i.e.* (Si–OH–Al), (P–OH) and OH groups associated with the extra-framework Al by nitrite groups. The bands at 3677 cm^{-1}, 3620 cm^{-1} and 3600 cm^{-1} might be assigned to the generation of O–H bond in the nitrite groups (–N–O–H) in different chemical environments.

As shown in Fig. 8b, when NH_3 introduced into the system, the bands associated with nitrite groups decreased rapidly. Before 5 minutes when there was an obvious decrease for bands assigned to nitrite groups, there was no bands belonging to adsorbed NH_3, this might suggest that NH_3 moved fast on surface that they reacted with the nitrite groups and did not accumulate, and some of the groups on the surface of the samples might take the role of transferring ammonia groups to active sites.

3.8.2 NH_3 adsorption and subsequent reaction with NO. As shown in Fig. 8c, after NH_3 introduced into the system, the band at 1456 cm^{-1} increased rapidly due to the generation of NH_3 species on BrØnsted acid sites,[8,30] and the growing band at 1210 cm^{-1} (not shown) was assigned to the generation of NH_3 species on Lewis acid though it was very weak. This indicates that most of the acid sites were from BrØnsted acid sites. The appearance of negative bands at 3592 cm^{-1}, 3629 cm^{-1} and 3674 cm^{-1} indicated the reducing of BrØnsted acid sites and the forming of NH_4^+ which was also supported by the band at 3283 nm^{-1} assigned to NH_4^+ groups.[7,9] Specifically, the negative band at 3674 cm^{-1} was assigned to the occupation of P–OH site by NH_3, which consequently reduced the corresponding OH stretching vibrations. The changes of other two bands were related to the depletion of Si–OH–Al acid site, which was also supported by the existing negative band at 2600 cm^{-1} attributed to the Si–OH–Al acid sites. The band at 3320–3550 cm^{-1} was attributed to N–H stretching vibrations of NH_4^+.[30] As shown in Fig. 8d, when NO introduced into the system, bands related to adsorbed NH_3

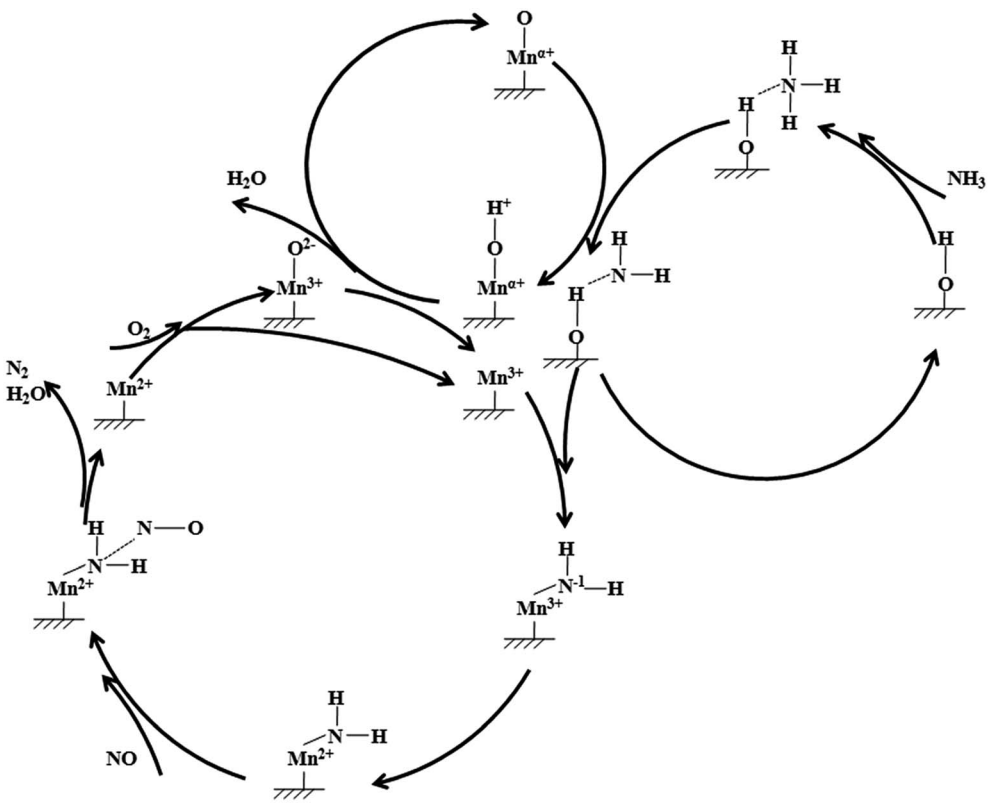

Fig. 9 The proposed low temperature SCR mechanism on 4Mn/SAPO-34.

species decreased gradually, this could be the evidence that BrØnsted acid sites and the NH_4^+ species were important to the low temperature SCR activity.

3.8.3 Reactions between NO and NH_3 under SCR reaction condition. Fig. 8e was similar to Fig. 8c that only NH_3 related bands were visible, any evidence of NO related bands did not appear especially the negative bands at 2700 and 3000–3400 cm^{-1}. It could be deduced that there is a great opportunity that the SCR reaction mechanism on the 4Mn/SAPO-34 at 150 °C was Eley–Rideal mechanism, since if Langmuir–Hinshelwood mechanism were effective, many NO would have been adsorbed on the surface due to the accumulation of NO species of which only the well activated parts had the appropriate energy to react with activated NH_3. In this case the negative bands at 2700 and 3000–3400 nm^{-1} would appear, as Fig. 8a and b suggested. As these peaks were not shown in Fig. 8e, all these observations lead to the exclusion of Langmuir–Hinshelwood mechanism and the assurance of Eley–Rideal mechanism.

From the evidence above, a mechanism for low temperature SCR reaction might be figured out. Fig. 9 showed the proposed low temperature SCR mechanism on 4Mn/SAPO-34. Firstly, NH_3 was adsorbed on the BrØnsted acid sites of SAPO-34, and then interacted with the adjacent manganese oxides. After one of the hydrogen of NH_3 captured by $Mn^{\alpha+}$–O^{2-}-like species, the remaining NH_2^{-1} species was transferred to Mn^{3+} ion and then oxidized to NH_2, *i.e.* the electron from NH_2^{-1} was captured by Mn^{3+} ion. The NO molecule from gas phase attacked the NH_2 on Mn^{2+} ion and formed NH_2NO-like transition state and subsequently decomposed to N_2 and H_2O. The Mn^{2+} ion left was then oxidized by O_2 to Mn^{3+} and Mn^{3+}–O^{2-}-like species which further reacted with $Mn^{\alpha+}$–O^{2-}-H-like species to Mn^{3+}.

4. Conclusions

For Mn/SAPO-34 catalyst, as Mn loading increased from 1% to 8%, the UV-Vis and H_2-TPR results indicated that the main Mn species in the zeolite channels changed from Mn^{2+} to Mn^{3+} or/and Mn^{4+}, the XPS showed that the main Mn species on the outer surface were Mn^{3+} and Mn^{4+} as the results of MnO_x aggregation on the extra-framework of SAPO-34.

The increased catalytic activity when Mn loading increased from 1% to 2% might be ascribed to the increase of Mn^{3+} or/and Mn^{4+} oxides of the outer surface since Mn^{3+} and Mn^{4+} species were mainly responsible for the low-temperature selective catalytic reduction activity. The higher SCR reaction activity of 4Mn/SAPO-34 and 8Mn/SAPO-34 was the result of the higher content of Mn^{3+} and Mn^{4+} species as compared with 2Mn/SAPO-34 and 1Mn/SAPO-34. The lack of exposed Mn oxides caused by aggregation and the BrØnsted acid sites on 8Mn/SAPO-34 as indicated by XRD and NH_3-TPD profile led to the lower catalytic activity compared with 4Mn/SAPO-34.

From the DRIFTS results, it could be deduced that NH_3 was mainly adsorbed on the BrØnsted acid, and the main mechanism on 4Mn/SAPO-34 at low temperature was Eley–Rideal mechanism, *i.e.* NO molecule from gas phase directly reacted with the well activated NH_3 species adsorbed on the surface and leaf as products to gas phase with the active site left.

Acknowledgements

This research is sponsored by China National Key Research and Development Program *via* Project No. 2016YFB0600603.

References

1 G. Qi and R. T. Yang, Performance and kinetics study for low-temperature SCR of NO with NH_3 over MnO_x–CeO_2 catalyst, *J. Catal.*, 2003, **217**, 434–441.
2 Z. Liua, Y. Yi, S. Zhang, T. Zhu, J. Zhu and J. Wang, Selective catalytic reduction of NO_x with NH_3 over Mn–Ce mixed oxide catalyst at low temperatures, *Catal. Today*, 2013, **216**, 76–81.
3 Z. Liu, J. Zhu, J. Li, L. Ma and S. I. Woo, Novel Mn–Ce–Ti Mixed-Oxide Catalyst for the Selective Catalytic Reduction of NO_x with NH_3, *ACS Appl. Mater. Interfaces*, 2014, **6**, 14500–14508.
4 Z. Liu, Y. Liu, Y. Li, H. Su and L. Ma, WO_3 promoted Mn–Zr mixed oxide catalyst for the selective catalytic reduction of NO_x with NH_3, *Chem. Eng. J.*, 2016, **283**, 1044–1050.
5 B. Thirupathi and P. G. Smirniotis, Nickel-doped Mn/TiO_2 as an efficient catalyst for the low-temperature SCR of NO with NH_3: Catalytic evaluation and characterizations, *J. Catal.*, 2012, **288**, 74–83.
6 J. J. Xue, X. Q. Wang, G. S. Qi, J. Wang, M. Q. Shen and W. Li, TiO_2-supported metal oxide catalysts for low-temperature selective catalytic reduction of NO with NH_3: I. Evaluation and characterization of first row transition metals, *J. Catal.*, 2013, **297**, 56–64.
7 L. Wang, W. Li, S. J. Schmieg and D. Weng, Role of Brønsted acidity in NH_3 selective catalytic reduction reaction on Cu/SAPO-34 catalysts, *J. Catal.*, 2015, **324**, 98–106.
8 D. Wang, L. Zhang, K. Kamasamudram and W. S. Epling, *In situ*-DRIFTS Study of Selective Catalytic Reduction of NO_x by NH_3 over Cu-Exchanged SAPO-34, *ACS Catal.*, 2013, **3**, 871–881.
9 M. Devadas, O. Kröcher, M. Elsener, A. Wokaun, N. Söger, M. Pfeifer, Y. Demel and L. Mussmann, Influence of NO_2 on the selective catalytic reduction of NO with ammonia over Fe-ZSM_5, *Appl. Catal., B*, 2006, **67**, 187–196.
10 A. Grossale, I. Nova, E. Tronconi, D. Chatterjee and M. Weibel, The chemistry of the NO/NO_2–NH_3 "fast" SCR reaction over Fe-ZSM_5 investigated by transient reaction analysis, *J. Catal.*, 2008, **256**, 312–322.
11 M. Iwasaki and H. Shinjoh, A comparative study of "standard", "fast" and "NO_2" SCR reactions over Fe/zeolite catalyst, *Appl. Catal., A*, 2010, **390**, 71–77.
12 S. Alexander, C. Per-Anders, H. Hanna and S. Magnus, Effect of preparation procedure on the catalytic properties of Fe-ZSM-5 as SCR catalyst, *Top. Catal.*, 2013, **56**(9–10), 567–575.
13 F. Gao, E. D. Walter, E. M. Karpl, J. Y. Luo, R. G. Tonkyn, J. H. Kwak, J. Szanyi and C. H. F. Peden, Structure-activity relationships in NH_3-SCR over Cu-SSZ-13 as probed by reaction kinetics and EPR studies, *J. Catal.*, 2013, **300**, 20–29.
14 L. Ma, Y. Cheng, G. Cavataio, R. W. McCabe, L. Fu and J. Li, Characterization of commercial Cu-SSZ-13 and Cu-SAPO-34

catalysts with hydrothermal treatment for NH_3-SCR of NO_x in diesel exhaust, *Chem. Eng. J.*, 2013, **225**, 323–330.

15 B. Shen, H. Ma and Y. Yao, Mn–CeO_x/Ti–PILCs for selective catalytic reduction of NO with NH_3 at low temperature, *J. Environ. Sci.*, 2014, **24**, 499–506.

16 A. L. Picone, S. J. Warrender, A. M. Z. Slawin, D. M. Dawson, S. E. Ashbrook and P. A. Wright, *etc.*, A co-templating route to the synthesis of Cu SAPO STA-7, giving an active catalyst for the selective catalytic reduction of NO, *Microporous Mesoporous Mater.*, 2011, **146**, 36–47.

17 R. Martínez-Franco, M. Moliner, P. Concepcion, J. R. Thogersen and A. Corma, Synthesis, characterization and reactivity of high hydrothermally stable Cu-SAPO-34 materials prepared by ''one-pot'' processes, *J. Catal.*, 2014, **314**, 73–82.

18 D. Wang, L. Zhang, J. H. Li, K. Kamasamudram and W. S. Epling, NH_3-SCR over Cu/SAPO-34 – Zeolite acidity and Cu structure changes as a function of Cu loading, *Catal. Today*, 2014, **231**, 64–74.

19 M. A. Zanjanchi and M. K. Rashidi, Structural charge transfer in the aluminophosphate molecular sieves by diffuse reflectance spectroscopy, *Spectrochim. Acta, Part A*, 1999, **55**, 947–954.

20 T. Kharlamova, G. Mamontov, M. Salaev, V. Zaikovskii, G. Popova, V. Sobolev, A. Knyazev and O. Vodyankina, Structural charge transfer in the aluminophosphate molecular sieves by diffuse reflectance spectroscopy, *Appl. Catal., A*, 2013, **467**, 519–529.

21 Q. Tang, S. Hu, Y. Chen, Z. Guo, Y. Hu, Y. Chen and Y. Yang, Highly dispersed manganese oxide catalysts grafted on SBA-15: Synthesis, characterization and catalytic application in *trans*-stilbene epoxidation, *Microporous Mesoporous Mater.*, 2010, **132**, 501–509.

22 I. Spassova, T. Tsontcheva, N. Velichkova, M. Khristova and D. Nihtianova, Catalytic reduction of NO with decomposed methanol on alumina-supported Mn–Ce catalysts, *J. Colloid Interface Sci.*, 2012, **374**, 267–277.

23 Z. Qu, Y. Bu, Y. Qin, Y. Wang and Q. Fu, The improved reactivity of manganese catalysts by Ag in catalytic oxidation of toluene, *Appl. Catal., B*, 2013, **132–133**, 353–362.

24 D. A. Peña, B. S. Uphade and P. G. Smirniotis, TiO_2-supported metal oxide catalysts for low-temperature selective catalytic reduction of NO with NH_3: I. Evaluation and characterization of first row transition metals, *J. Catal.*, 2004, **221**, 421–431.

25 C. Norsic, J.-M. Tatibouët, C. Batiot-Dupeyrat and E. Fourré, Non thermal plasma assisted catalysis of methanol oxidation on Mn, Ce and Cu oxides supported on γ-Al_2O_3, *Chem. Eng. J.*, 2016, **304**, 563–572.

26 B. R. Strohmeier and D. M. Hercules, Surface spectroscopic characterization of manganese/aluminum oxide catalysts, *J. Phys. Chem.*, 1984, **88**, 4922–4929.

27 M. H. Groothaert, K. Lievens, H. Leeman, B. M. Weckhuysen and R. A. Schoonheydt, An operando optical fiber UV–vis spectroscopic study of the catalytic decomposition of NO and N_2O over Cu-ZSM-5, *J. Catal.*, 2003, **220**, 500–512.

28 C. Lamberti, S. Bordiga, M. Salvalaggio, G. Spoto and A. Zecchina, XAFS, IR, and UV-Vis Study of the Cu^I Environment in Cu^I-ZSM-5, *J. Phys. Chem. B*, 1997, **101**, 344–360.

29 M. Iwasaki and H. Shinjoh, NO evolution reaction with NO_2 adsorption over Fe/ZSM-5: *In situ* FT-IR observation and relationships with Fe sites, *J. Catal.*, 2010, **273**, 29–38.

30 J. Y. Luo, H. Oh, C. Henry and W. Epling, Effect of C_3H_6 on selective catalytic reduction of NO_x by NH_3 over a Cu/zeolite catalyst: A mechanistic study, *Appl. Catal., B*, 2012, **123–124**, 296–305.

